ARTICLE

Macrophages and glia are the dominant P2X7-expressing cell types in the gut nervous system—No evidence for the role of neuronal P2X7 receptors in colitis

Tina Jooss [1,†], Jiong Zhang [1,†,‡], Béla Zimmer [1], Tanja Rezzonico-Jost [2], Björn Rissiek [3], Penelope Felipe Pelczar [4], Frauke Seehusen [5], Friedrich Koch-Nolte [6], Tim Magnus [3], Susanna Zierler [1,7], Samuel Huber [4], Michael Schemann [8], Fabio Grassi [2] and Annette Nicke [1,✉]

The blockade or deletion of the pro-inflammatory P2X7 receptor channel has been shown to reduce tissue damage and symptoms in models of inflammatory bowel disease, and P2X7 receptors on enteric neurons were suggested to mediate neuronal death and associated motility changes. Here, we used P2X7-specific antibodies and nanobodies, as well as a bacterial artificial chromosome transgenic P2X7-EGFP reporter mouse model and *P2rx7*$^{-/-}$ controls to perform a detailed analysis of cell type-specific P2X7 expression and possible overexpression effects in the enteric nervous system of the distal colon. In contrast to previous studies, we did not detect P2X7 in neurons but found dominant expression in glia and macrophages, which closely interact with the neurons. The overexpression of P2X7 *per se* did not induce significant pathological effects. Our data indicate that macrophages and/or glia account for P2X7-mediated neuronal damage in inflammatory bowel disease and provide a refined basis for the exploration of P2X7-based therapeutic strategies.

Mucosal Immunology (2023) 16:180–193; https://doi.org/10.1016/j.mucimm.2022.11.003

INTRODUCTION

Inflammatory bowel diseases (IBDs), such as ulcerative colitis and Crohn's disease, are chronic relapsing-remitting inflammatory diseases with rising incidence in industrialized countries. They are thought to result from an abnormal host-microbial response of the intestinal immune system in a genetically susceptible host[1,2]. The resulting imbalance of homeostatic immunomodulatory mechanisms is characterized by increased macrophage and T-cell activation and upregulation of pro-inflammatory cytokines[3,4]. In addition, IBDs are associated with enteric neurodegeneration and abnormal gut motility, and the resulting breakdown of enteric nervous system (ENS) control is a major contributing factor in the development of functional bowel disorders[5–7].

Extracellular purines play important roles in immune cell regulation and enteric signaling[8–12]. High concentrations of adenosine triphosphate (ATP) are sensed as a danger signal by the P2X7 receptor, and it is generally accepted that activation of this nonspecific cation channel acts as a secondary stimulus to induce NLRP3 inflammasome assembly and subsequent maturation and release of pro-inflammatory interleukin (IL)-1β from macrophages. In addition, it has been shown that ATP, through the P2X7 receptor, induces apoptosis in several cell types[13–16]. Although the pathophysiological roles of P2X7 receptors have been well established in *P2rx7*$^{-/-}$ mouse models[17,18], possible physiological roles are comparably poorly investigated.

The expression of P2X7 was shown to be increased in patients with IBD and animal models, and its deletion or blockade reduced tissue damage in different rodent colitis models[12,19,20]. In a short phase IIa clinical study with a limited number of patients, oral application of a P2X7 antagonist ameliorated the pain component in the Crohn's disease activity index but did not change the biomarkers of inflammation[21].

A variety of cell types in the colon have been shown to express P2X7 receptors and were involved in colitis pathology. These include immune cells, such as mast cells[22–24], and different types of T cells[25,26], epithelial cells[27–29], and enteric neurons of both the submucosal and myenteric plexus[5,20,30–32]. P2X7-mediated neuronal cell death was implicated in motor dysfunction associated with colitis[5,30–33]. Accordingly, elevated levels of extracellular ATP chronically activate a neuronal P2X7/Pannexin/Asc/caspase complex that leads to preferential loss of nitrergic neurons[5]. Although numerous mechanisms and cell types have been proposed to mediate protective effects of P2X7 blockade, the localization of P2X7 receptors in specific cell types *in situ* has

[1]Walther Straub Institute of Pharmacology and Toxicology, Faculty of Medicine, Ludwig Maximilian University, Munich, Germany. [2]Institute for Research in Biomedicine, Faculty of Biomedical Sciences, Università della Svizzera Italiana, Bellinzona, Switzerland. [3]Department of Neurology, University Medical Center Hamburg-Eppendorf, Hamburg, Germany. [4]Department of Medicine, University Medical Center Hamburg-Eppendorf, Hamburg, Germany. [5]Laboratory for Animal Model Pathology (LAMP), Institute of Veterinary Pathology, Vetsuisse Faculty, University of Zurich, Zurich, Switzerland. [6]Institute of Immunology, University Medical Center Hamburg-Eppendorf, Hamburg, Germany. [7]Institute of Pharmacology, Medical Faculty, Johannes Kepler University Linz, Linz, Austria. [8]Human Biology, Technical University Munich, Freising-Weihenstephan, Germany. ✉ email: annette.nicke@lrz.uni-muenchen.de. † Both authors equally contributed. ‡ Present address: Institute of Pathophysiology, University Medical Center of the Johannes, Gutenberg University Mainz, Mainz, Germany.

Received: 23 November 2022 Accepted 29 November 2022
Published online: 10 January 2023

been challenging due to a lack of metabolically stable and selective pharmacological tools. In addition, the specificity of the used antibodies has not been demonstrated in most studies. So far, the role of P2X7 receptors in neurons remains unclear; however, its cell type-specific expression, in neurons versus immune cells in particular, has important implications for potential treatments. In this study, we therefore set out to perform a detailed analysis of P2X7-expressing cell types in the distal colon using a bacterial artificial chromosome (BAC) transgenic P2X7-EGFP reporter mouse model[34] in combination with a P2X7-selective nanobody and *P2rx7*$^{-/-}$ mice as the negative control.

MATERIAL AND METHODS

Animals

BAC transgenic P2X7-EGFP mice [Tg(RP24-114E20P2X7451P-StrepHis-EGFP)Ani15 and 17] were recently described[34] and in FVB/N or C57BL6 background. Identical P2X7 expression patterns were observed in both lines and strains. *P2rx7*$^{-/-}$ mice [P2rx7$^{tmid(EUCOMM)Wtsi}$] were bred as described in a study by Kaczmarek-Hajek et al.[34] and in C57BL/6 background. Animals aged 12–18 weeks of both sexes were used. Mice were housed in standard conditions (22°C, 12-hour light-dark cycle, water/-food *ad libitum*). All animal experiments were performed in accordance with the principles of the European Communities Council Directive (2010/63/EU). The procedures were reviewed and approved by the State of Upper Bavaria (55.2-1-54-2532-59-2016). All efforts were made to minimize suffering and limit the number of animals.

Flow cytometric analysis

For the purification of leukocytes from the large intestine, the colon was separated from the small intestine, opened by longitudinal section, and feces was washed out thoroughly in the Hanks balanced salt solution. The cleaned colon was cut into 1-cm pieces and further washed in 20-ml Hanks balanced salt solution at 37°C for 30 minutes. Colon pieces were then digested for 30 minutes at 37°C in a digestion solution containing collagenase (1 mg/ml) and DNase (0.1 mg/ml). The generated cell suspension was filtered through a 100-µm cell strainer and centrifuged for 5 minutes at 300 g. Leukocytes were separated from debris by resuspending the pellet in 5 ml 33% Percoll solution (GE Healthcare, Chicago, IL, USA). Erythrocytes were lyzed using an ammonium-chloride-potassium lysis buffer (155 mM NH_4Cl, 10 mM $KHCO_3$, 0.1 mM EDTA, pH 7.2). Isolated cells were stained with an antibody mix in fluorescent activated cell sorting buffer [containing 1 mM EDTA and 0.1 % bovine serum albumin (both from Sigma-Aldrich, St. Louis, MO, USA)] for 30 minutes at 4°C (for antibodies, see key resource table) to identify major immune cell populations, including T cells and innate immune cells. Cells were washed once with fluorescent activated cell sorting buffer and were subsequently analyzed on a Becton Dickinson FACSymphony A3 cell analyzer (Becton Dickinson, Franklin Lakes NJ, USA).

Whole-mount myenteric plexus and submucosal plexus preparation from the distal colon

For the whole-mount myenteric plexus and submucosal plexus preparation, the mice were sacrificed by cervical dislocation and 1-cm segments were taken 1 cm aboral from the proximal colon and transferred to ice-cold Krebs solution (containing in mM: 117 NaCl, 4.7 KCl, 1.2 $MgCl_2$, 1.2 NaH_2PO_4, 25 $NaHCO_3$, 2.5 $CaCl_2$, 11 glucose, aerated with carbogen to pH 7.4) in Sylgard (Dow Corning, Midland MI, USA)-filled dissecting dishes. After flushing with the Krebs buffer, segments were opened along the mesenteric border, pinned out, and fixed for 4 hours at 4° C [4% paraformaldehyde (PFA) and 0.2% picric acid in 0.1 M phosphate buffer (pH 7.4)]. Tissue was rinsed (3 × 10 minutes) with phosphate buffer and dissected in phosphate-buffered saline (PBS; pH 7.4). Using forceps and a stereomicroscope, the mucosa and submucosa were carefully removed. For myenteric plexus preparations, the circular musculature was also removed. Submucosal and myenteric plexus reparations were transferred to a reaction tube with blocking buffer [0.5% Triton X-100, 0.1% NaN_3, 4% goat serum (Sigma-Aldrich, St. Louis, MO, USA) in PBS] and after 1 hour at room temperature (RT), incubated with primary antibodies in blocking buffer (12 hours at RT), washed 3 × 10 minutes with PBS, and incubated with secondary antibodies (2 hours at RT). After a final washing step (3× in PBS) preparations were mounted in PermaFluor (Thermo Fisher Scientific, Waltham, MA, USA) on slides. All antibodies are indicated in the Supplementary Table 1.

Image acquisition and processing

Fluorescent images were taken with a Leica SP5 (Leica, Wetzlar, Germany) or Zeiss LSM 880 Airyscan (Carl Zeiss AG, Oberkochen, Germany) confocal microscope at ×20, ×40, or ×63 magnification using LAS AF (Leica, Wetzlar, Germany) or Zen blue 2.3 software (Carl Zeiss AG, Oberkochen, Germany). The pinhole was set to 1 AU for each channel to ensure that only fluorescence that originates from the focal point is captured by the detector. Z-stack images were acquired at 1-µm intervals to obtain the final depth of 5–10 µm. To minimize fluorescence crosstalk, channels were acquired sequentially with the spectral slit adjusted for each respective emission wavelength. For an initial comparison of WT, P2X7 knockout, and transgenic P2X7 mice, tissues were processed in parallel and identical parameters for image acquisition [laser intensity, pinhole, detector gain, pixel time, line time, scaling per pixel, image size (1024 × 1024), averaging] were used and settings were chosen to determine specific staining in WT animals. To prevent saturation in transgenic animals and visualize faint background structures in knockout animals, the brightness was adjusted by reducing or increasing the microscope detector gain, respectively. Specific staining observed in WT animals served as a reference for the preparation of images that were prepared without knockout controls. Raw 8-bit grayscale images were imported into ImageJ and opened as single images or stacks. The Z-project function was used to select the first and last slices of the projection and maximum intensity was chosen as projection type. Merged images were saved as TIFF files. In some cases, the brightness was further adjusted in ImageJ to improve the visibility of structures.

Preparation and staining of colon cryosections

Animals were anesthetized with isoflurane (IsoFlo, Abbott Laboratories, Chicago, IL, USA) and euthanized by cervical dislocation. The distal colon was prepared, flushed three times with PBS, embedded in Tissue Tek (Sakura Finetek, Alphen aan den Rijn, Netherlands), and after freezing at −80°C, cut in 10-µm cross-sections using a Cryostat Microm HM560 (Leica Biosystems, Wetzlar, Germany).

For immunofluorescence staining, distal colon sections were dried for 1 hour at RT, fixed for 20 minutes (2% PFA in 150 mM sodium phosphate buffer pH 7.4), and washed 2 × 10 minutes

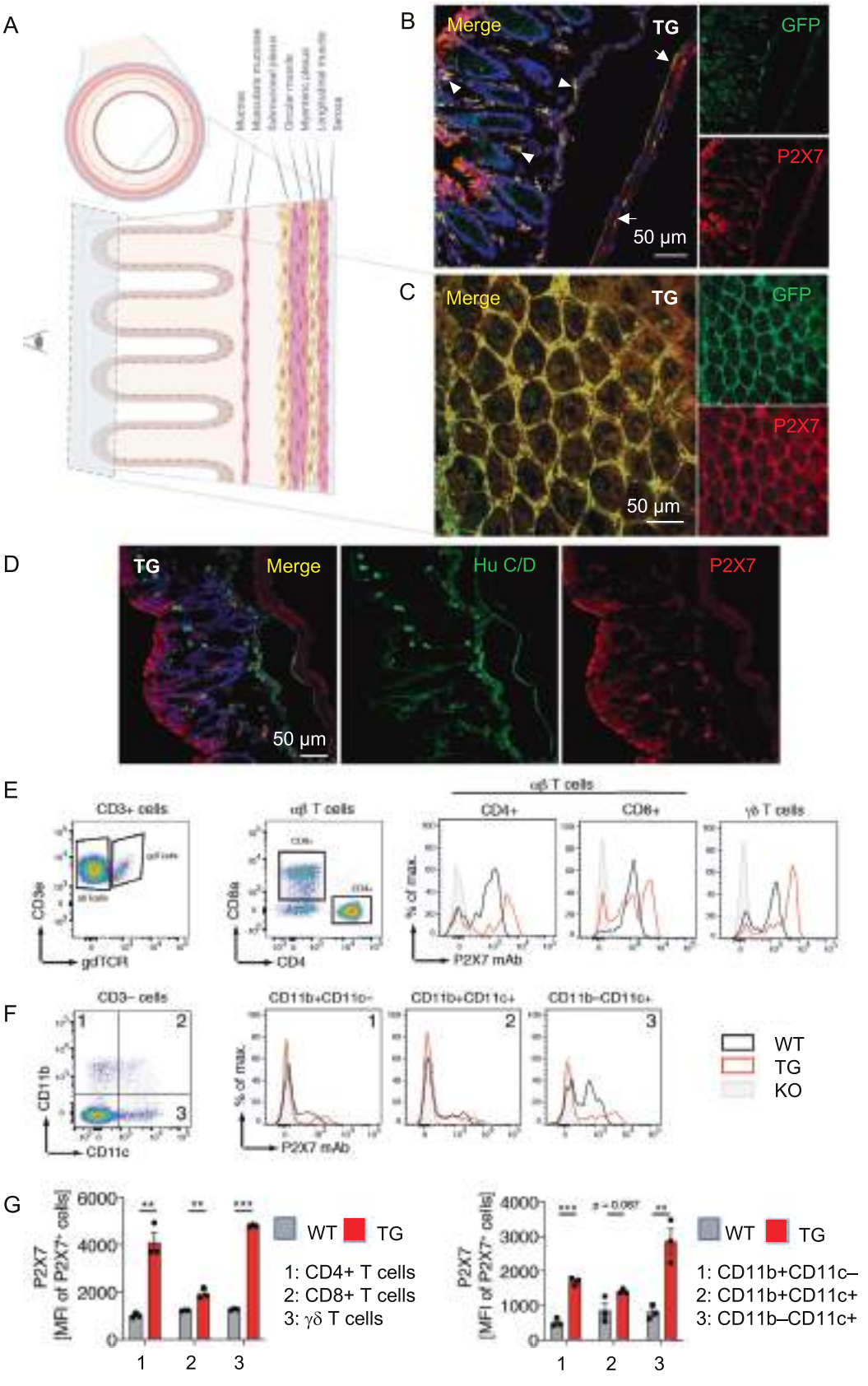
A
B
Merge
TG
GFP
P2X7
50 µm
C
Merge
TG
GFP
P2X7
50 µm
D
TG
Merge
50 µm
Hu C/D
P2X7
E
CD3+ cells
αβ T cells
αβ T cells
CD4+
CD8+
γδ T cells
CD3e
gdTCR
CD8a
CD4
% of max.
P2X7 mAb
F
CD3− cells
CD11b+CD11c−
CD11b+CD11c+
CD11b−CD11c+
CD11b
CD11c
% of max.
P2X7 mAb
WT
TG
KO
G
P2X7 [MFI of P2X7+ cells]
WT
TG
1: CD4+ T cells
2: CD8+ T cells
3: γδ T cells
P2X7 [MFI of P2X7+ cells]
WT
TG
1: CD11b+CD11c–
2: CD11b+CD11c+
3: CD11b–CD11c+

with PBS and 1 × 10 minutes with water. After drying at RT, slices were blocked for 1 hour (10% goat serum, 0.5% Triton X-100, in PBS, pH 7.4) and then incubated overnight at 4°C with 100 µl of the primary antibody dilution in blocking solution using a humid chamber.

After washing (3 × 10 min in PBS), 100 µl of the secondary antibody dilution in blocking buffer was applied for 1 hour at RT and slices were then washed (2 × 10 minutes with PBS, 1 × 10 minutes with water). The sections were subsequently treated for 1 minute with 0.1% 4′,6-diamidino-2-phenylindole (DAPI), washed 3 × 5 minutes with PBS, and embedded in the Perma-Fluor Mounting Medium (Epredia, Kalamazoo, MI, USA). The preparations were analyzed using a Zeiss 880 Airyscan (Carl Zeiss AG, Oberkochen, Germany) confocal microscope. For antibodies, see Supplementary Table 1.

Counting analysis

For the counting analysis, 1-cm^2 whole-mount LMMP preparations taken 1 cm aboral from the beginning of distal colon were used. Five and 10 z-stack images (0.25 mm^2 for macrophages and 0.5 mm^2 for neurons) were randomly selected for counting of macrophages or neurons, respectively. Only F4/80-positive macrophages or HuCD-positive neurons that were completely within the image were counted using the ImageJ point tool.

Benzoyl-ATP treatment

For *ex vivo* benzoyl-ATP treatment of LMMP preparations, a modified protocol from a study by Gulbransen et al.[5] was used. The distal colon was prepared, mounted with minutien pins in a Sylgard dish, and opened along the mesenteric border as described previously. The mucosa, submucosa, and submucosal plexus were prepared off the muscle layer. The circular muscle layer was maintained to avoid shearing stress of the MP. The tissue was then incubated for 1 hour in a cell culture incubator with 20 ml of 300 µM BzATP in the Krebs buffer (containing in mM: 117 NaCl, 4.7 KCl, 1.2 $MgCl_2$, 1.2 NaH_2PO_4, 25 $NaHCO_3$, 2.5 $CaCl_2$, 11 glucose, aerated with carbogen to pH 7.4). The tissue was then washed 3 × 10 minutes with the Krebs buffer and incubated for another 2 hours with 20-ml Krebs buffer before fixation for 4 hours [4% paraformaldehyde (PFA) and 0.2% picric acid in 0.1 M of phosphate buffer (pH 7.4)] at 4°C. Subsequently, the circular muscle layer was removed, and immunofluorescence staining was performed as described previously.

Dextran sulfate sodium (DSS) colitis model

BAC transgenic P2X7-EGFP mice [Tg(RP24-114E20P2X7451P-Stre pHis-EGFP)Ani17][34] and their WT control littermates were acclimatized for at least 7 days and maintained and treated in accordance with the Swiss Federal Veterinary Office guidelines of the institutional review board of the animal facility. Experiments were approved by *Dipartimento della Sanitá e Socialitá*, with authorization number 29172 (TI-25/2018, TI-24/2019, and TI-20/2021) and 33486 (TI 20/2021). All mice were from the same rack and room and housed in standard conditions (20–22°C, 12-hour light-dark cycle, water/food *ad libitum* in cages with environmental enrichment, such as tunnel and pressed cotton squares for nest building). The mice were monitored and weighted daily (not blinded). For experimental procedures (based on experience and with help of Clin Calc Simple Size Calculator between two independent study groups, namely WT DSS and TG DSS, with continuous primary end point), 35 female mice (16 weeks old) were used and randomly allocated as indicated. No animals were excluded. Six untreated mice (3 WT and 3 TG) of the same sex and age were added to colon length statistic. The following values were used to establish the daily fecal score: 0, normal solid feces; 1, soft feces; 2, liquid feces; and 3, visible blood traces on feces. All efforts were made to minimize suffering and limit the number of animals used in experiments.

DSS (TdB LabsAB, Uppsala, Sweden) was added at a concentration of 1% in drinking water for 6 days. Then, DSS 1% was replaced with normal drinking water for the other 4 days. After 10 days from the beginning of the experiment, the mice were sacrificed by inhalation of CO_2 for the retrieval of organs.

The histological analysis was performed in a blinded way according to Dieleman et al.[67]. Briefly, a range from 0–3 was used to describe the amount of and depth of inflammation. Furthermore, a range from 0–4 described the amount of crypt damage and regeneration. These changes were also quantified as to the percentage of tissue involvement (1 = 1%–25%, 2 = 26%–50%, 3 = 51%–75%, 4 = 76%–100%). Each section was then scored for each feature separately by establishing the product of the grade for that feature and the percentage involvement (in a range from 0–12 for inflammation and for extent and in a range from 0–16 for regeneration and for crypt damage).

Statistical analysis

The GraphPad Prism (version 9) software was used for statistical analysis and data were presented as means ± standard derivation (SD). Student's t test, Mann-Whitney-U test, and one-way

Fig. 1 P2X7 localization in different layers and immune cell types of the mouse distal colon. A, Schematic drawing (created with BioRender.com) of the histological structure of the colon explaining the cell layers and perspectives of the images shown in (B-D). B, Co-staining of colonic cross section and a planar mucosa preparation. C, from P2X7-EGFP mice with anti-P2X7 and anti-GFP antibodies. Arrow heads and arrows in (B) indicate examples of single cells and layers with clear co-localization. (D) Co-staining of colonic cross section with anti-P2X7 antibodies and an antibody against the neuronal marker HuC/D. <scale bar: 50 µm>, cell nuclei were counterstained with 4′,6-diamidino-2-phenylindole (DAPI, blue). E, Flow cytometric analyses of colonic immune cells from WT (black), P2X7-EGFP transgenic (red), and *P2rx7*$^{-/-}$ mice (gray). Within the $CD3^+$ T-cell population, $CD4^+$ and $CD8^+$ αβ T cells and γδ T cells were analyzed for cell surface P2X7 expression using the mAb RH23A44. The right-shifted histogram indicates higher P2X7 expression in transgenic mice. F, Comparison of P2X7 expression in innate immune cells. Among $CD3^-$ innate immune cells, $CD11b^+CD11c^-$, $CD11b^+CD11c^+$, and $CD11b^-CD11c^+$ cells were analyzed for cell surface P2X7 expression using the monoclonal antibody RH23A44. G, Quantification of data from (E) and (F). P2X7 expression in $P2X7^+$ cells from P2X7-transgenic (red) and WT (dark) is shown (n = 3 / group, mean + SD, Student's t test, ** $p < 0.01$, *** $p < 0.001$). GFP = green fluorescent protein; KO =$P2X7^{-/-}$ mouse; TG = P2X7-EGFP transgenic mouse; WT = wild-type mouse.

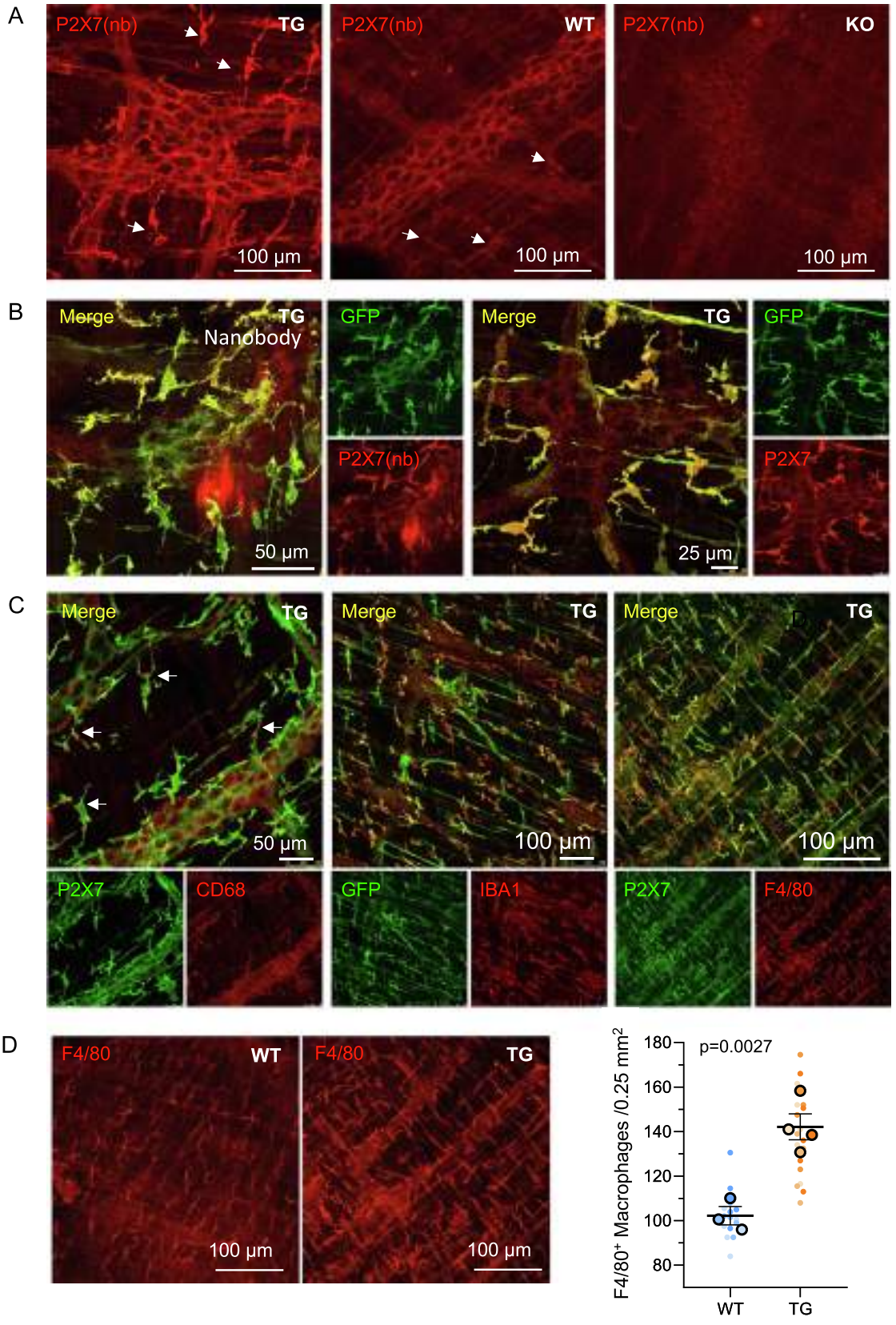
A
P2X7(nb)
TG
100 µm
P2X7(nb)
WT
100 µm
P2X7(nb)
KO
100 µm
B
Merge
TG
Nanobody
50 µm
GFP
P2X7(nb)
Merge
TG
25 µm
GFP
P2X7
C
Merge
TG
50 µm
Merge
TG
100 µm
Merge
TG
100 µm
P2X7
CD68
GFP
IBA1
P2X7
F4/80
D
F4/80
WT
100 µm
F4/80
TG
100 µm
F4/80+ Macrophages /0.25 mm2
p=0.0027
180
160
140
120
100
80
WT
TG

or two-way analysis of variance (Tukey multiple comparisons test) were used to determine statistical differences between groups, as indicated in the legends. Significance was accepted at * p value < 0.05, ** p value < 0.01 ***, and p value < 0.001.

RESULTS

Expression of P2X7 and P2X7-EGFP in different layers and cell types of the colon

To determine the localization of P2X7 across the different layers of the colon, we first analyzed cross-sections of the distal colon in the P2X7-EGFP transgenic mouse model[34] (Figs 1A and 1B). In this mouse, an EGFP-tagged P2X7 receptor is overexpressed under the control of BAC-derived P2X7 promoters. The respective BAC contains the full-length *P2rx7* gene flanked by about 100 kb and 10 kb upstream and downstream sequences, respectively, and careful analysis of P2X7-EGFP localization in the central nervous system (CNS) has previously confirmed a P2X7-EGFP expression pattern that is identical to the endogenous P2X7 receptor and revealed predominant expression in microglia, oligodendrocytes, and Bergmann glia[34]. Co-staining of colon slices with antibodies against GFP and P2X7 revealed good co-localization of both signals in single cells throughout the lamina propria (arrowheads in Fig. 1B) and in two distinct layers adjacent to and in the muscular layer (arrows in Fig. 1B). The cells in the lamina propria show more intense staining and most likely represent macrophages based on their size, morphology, and localization, which is in agreement with the known high P2X7 expression in this cell type[14]. A weaker EGFP staining and more intense signal of the P2X7 antibody was seen in the apical side of the mucosa. Because the anti-P2X7 antibody should detect both P2X7-EGFP and endogenous P2X7, this could indicate a lower expression of the P2X7-EGFP protein in enterocytes, which would be in agreement with the dynamic regulation of P2X7 expression in epithelial cells[28]. Alternatively, unspecific staining or higher background signal of the P2X7 antibody in these cells or in this preparation could account for the difference. To further confirm the expression of epithelial P2X7-EGFP, we also performed co-staining of P2X7-EGFP with an anti-P2X7 nanobody in planar mucosa preparations (Fig. 1C). This revealed an almost complete signal overlap, confirming a good correlation between P2X7-EGFP and endogenous P2X7 localization in epithelial cells. As the presence of P2X7 receptors in enteric neurons has been frequently reported[5,30–32], we next performed co-staining for P2X7 and the neuronal markers HuC/D (RNA-binding proteins HuC and HuD) to further determine the identity of the P2X7-expressing cells in the tunica muscularis (Fig. 1D). Although both P2X7 and HuC/D signals were present in the same layers, they were clearly separated, indicating localization in different cell types or different subcellular structures.

To compare the cell type-specific expression of P2X7 in immune cells of the colon from P2X7-EGFP transgenic and wild-type (WT) mice, we performed flow cytometry and stained immune cells isolated from the colon with an anti-P2X7 monoclonal antibody. Among T cells, cluster of differentiation (CD) 4^+, $CD8^+$, and γδ T cells from P2X7-EGFP transgenic and WT mice exhibited a similar P2X7 expression pattern, although cells from P2X7-EGFP transgenic mice showed a higher P2X7 level in general due to transgene overexpression (Fig. 1E). Similarly, colon-derived innate immune cells, differentiated by the expression of CD11b and CD11c, showed a comparable P2X7 expression pattern in P2X7-EGFP transgenic and WT mice. Here, P2X7 was expressed on CD11b+CD11c−, CD11b+CD11c+, and CD11b −CD11c+ cells (Fig. 1F). Again, the expression of P2X7 was higher in P2X7-expressing cells from P2X7-EGFP transgenic mice than that from WT mice (Fig. 1F).

P2X7 expression in macrophages of the myenteric plexus

To further investigate the expression of P2X7 in the muscular layer and identify the respective P2X7-expressing cell types, we next stained whole-mount preparations of the longitudinal muscle and myenteric plexus (LMMP) from the distal colon of P2X7-EGFP, WT, and *P2rx7*$^{-/-}$ mice with the P2X7-specific nanobody. This revealed specific staining of enteric ganglia that appeared as mesh-like structures and large isolated extraganglionar cells with ramified morphology (arrows in Fig. 2A, also compare Figs 3A and 5A). The staining of the latter was particularly strong in the P2X7-EGFP mice, which was confirmed by co-staining with an antibody against GFP (Fig. 2B). In contrast, the EGFP signal in the mesh-like structures was less consistent and had a patchy appearance, suggesting that EGFP was only present in some clusters of the cells that are forming this structure (compare 2 representative images in Fig. 2B and Fig. 4A, right panel). Co-staining with antibodies against F4/80 (EGF-like module-containing mucin-like hormone receptor-like 1); Iba1 (ionized calcium-binding adapter molecule 1, also known as allograft-inflammatory factor 1); and CD68 confirmed that the extraganglionar cells represent macrophages, which is in agreement with the known expression of P2X7 receptors in these cell types (Fig. 2C). Two different types of macrophages could be differentiated; macrophages with longitudinal orientation and bipolar morphology likely represent muscular macrophages, whereas those with ramified morphology were localized in the

Fig. 2 P2X7 staining in whole-mount LMMP preparations from the distal colon. A, Specificity of the P2X7-specific nanobody. Preparations from P2X7-EGFP (TG), wild-type (WT), and *P2rx7*$^{-/-}$ (KO) mice were stained as indicated and confocal images were taken with identical settings. Arrows indicate extraganglionar P2X7-positive cells. B, Two representative confocal images of preparations from P2X7-EGFP transgenic mice co-stained with anti-GFP (GFP) and anti-P2X7 (P2X7) antibody or nanobody (nb), as indicated. C, Tissues from P2X7-EGFP mice were co-stained with anti-P2X7 or anti-GFP antibodies and antibodies against different macrophage marker proteins. Arrows indicate examples of CD68-positive macrophages. D, Representative images of tissue from P2X7-EGFP and WT mice stained with an antibody against the macrophage marker F4/80 and statistical analysis of macrophage numbers in both genotypes. n = 5 images of 0.25 mm^2 from the distal colon were analyzed per mouse. Data are represented as mean ± SEM from N = 3–4 mice per group (large symbols). Numbers for individual mice are represented in small symbols with different color intensities for each mouse. 97.03 ± 12.91 and 202.7 ± 32.03 macrophages per image were counted in WT and transgenic mice, respectively. Statistical significance was tested by Welch's t test (p = 0.0027). Normal distribution (Shapiro-Wilk, Kolmogorov-Smirnov, QQ plot) was confirmed for each group.

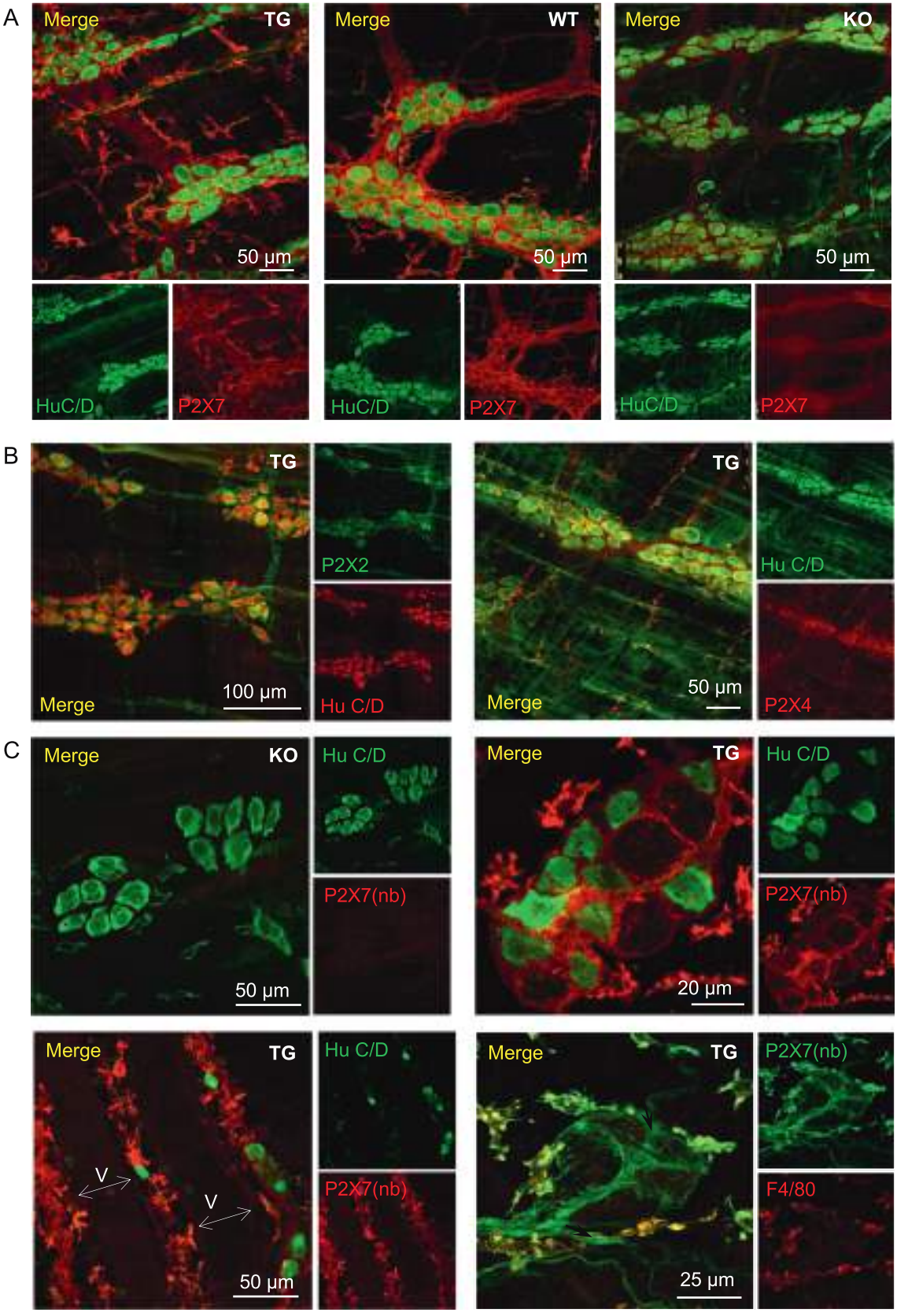
A
Merge
TG
50 µm
HuC/D
P2X7
Merge
WT
50 µm
HuC/D
P2X7
Merge
KO
50 µm
HuC/D
P2X7
B
TG
Merge
100 µm
P2X2
Hu C/D
TG
Merge
50 µm
Hu C/D
P2X4
C
Merge
KO
50 µm
Hu C/D
P2X7(nb)
Merge
TG
20 µm
Hu C/D
P2X7(nb)
Merge
TG
V
V
50 µm
Hu C/D
P2X7(nb)
Merge
TG
V
25 µm
P2X7(nb)
F4/80

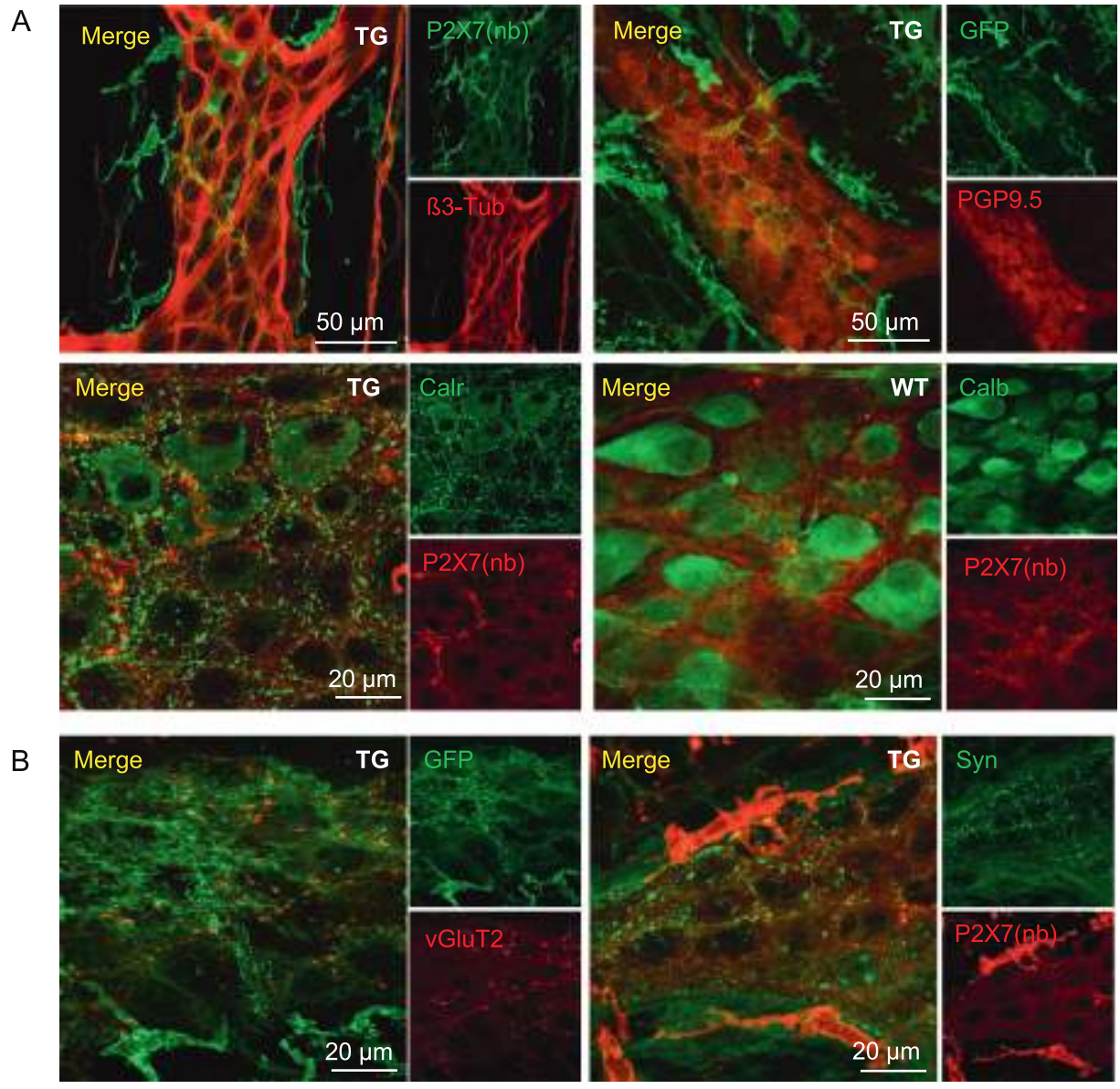

Fig. 4 Analysis of neuronal and synaptic P2X7 localization in whole-mount LMMP preparations from the distal colon. Tissues from P2X7-EGFP (TG) and wild-type (WT) mice were co-stained with P2X7-specific nanobody or anti-GFP antibodies as indicated and antibodies against different neuronal (A) or synaptic (B) marker proteins. β3-Tub = β3-tubulin; Calr = Calretinin; Calb = Calbindin; GFP = green fluorescent protein; PGP9.5 = protein gene product 9.5; Syn = synaptophysin; vGluT2 = vesicular glutamate transporter 2; Additional staining in WT tissue is shown in Supplementary Fig. 5.

vicinity of ganglions. Interestingly, only the ramified macrophages were positive for Iba1 (see Supplementary Fig. 1A). Ramified macrophages were also positive for the proliferation marker Ki67 (Supplementary Fig. 1B), which is in agreement with the notion that macrophages in the myenteric plexus have the ability to maintain themselves[35]. Because macrophage numbers appeared to be increased in P2X7-EGFP mice in comparison to WT mice (Fig. 2D, also compare Fig. 3A), we performed a quan-

Fig. 3 Analysis of neuronal P2X7 localization in LMMP and submucosal plexus preparations from the distal colon. A, Specificity of staining with the P2X7-specific antibody in combination with antibodies against the neuronal marker HuC/D. LMMP preparations from P2X7-EGFP (TG), wild-type (WT), and *P2rx7*$^{-/-}$ (KO) mice are shown. B, Co-staining of HuC/D and P2X2 receptors or P2X4 receptors (both used as positive controls for neuronal P2X expression) in LMMP preparations from P2X7-EGFP mice. C, Co-staining of P2X7 (using the P2X7 nanobody) and HuC/D in submucosal plexus preparations of *P2rx7*$^{-/-}$ and P2X7-EGFP mice, as indicated (upper panel). The images from P2X7-EGFP mice demonstrate staining of ganglia (right panel) and blood vessels (arrows in lower left image). V indicates the lumen of the blood vessel. The lower right image confirms P2X7 co-staining with the macrophage marker F4/80. GFP = green fluorescent protein.

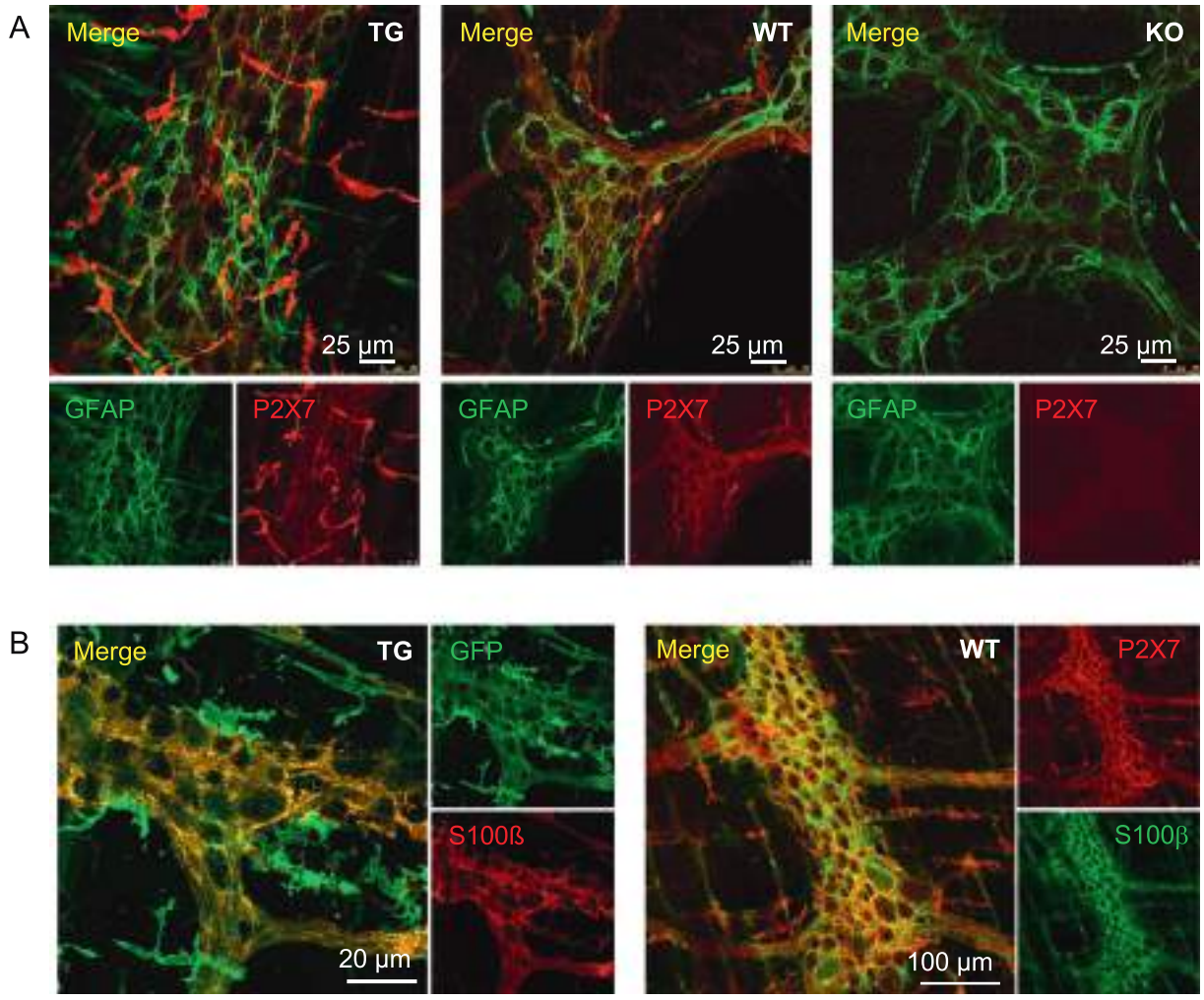

Fig. 5 Analysis of P2X7 localization in enteric glia of the myenteric plexus from distal colon. A, Specificity of staining with the P2X7-specific antibody in combination with antibodies against the glial marker glial fibrillary acidic protein GFAP (anti-GFAP antibody from mouse). LMMP preparations from P2X7-EGFP (TG), wild-type (WT), and *P2rx7*$^{-/-}$ (KO) mice are shown. Note that the weaker intensity of the ganglionic P2X7 signal in transgenic mice compared with WT mice is because of the fact that P2X7-EGFP overexpression is particularly strong in macrophages and the reduction of the signal intensity (to avoid saturation) consequently results in a weaker glia staining in transgenic mice. B, Co-staining of P2X7-EGFP (using the anti-GFP antibody) in tissue from P2X7-EGFP mice or P2X7 (using an anti-P2X7 antibody) in WT mice with the glial marker S100β. GFP = green fluorescent protein; GFAP = glial fibrillary acidic protein; S100β = S100 calcium-binding protein β.

titative analysis by counting the F4/80-positive macrophages in randomly chosen images of both genotypes. This revealed about 40% more macrophages in the myenteric plexus of P2X7-overexpressing mice than in Wt mice [102.2 ± 4.2 and 142.1 ± 5.8 standard error of the mean (SEM) macrophages per image (0.125 mm^2, n = 5 images/mouse) in WT (N = 3) and transgenic mice (N = 4), respectively]. Finally, co-staining with antibodies against Anoctamin-1 and CD117 excluded the presence of P2X7 receptors in myenteric interstitial cells of Cajal that function as pacemaker cells (Supplementary Fig. 2). The good correlation between the staining of Anoctamin-1 and CD117, which also represents a mast cell marker, is in agreement with a low number of mast cells in the myenteric plexus.

No evidence for P2X7 expression in neurons of the myenteric and submucosal plexuses

We next performed co-staining of HuC/D and P2X7 in the myenteric plexus (Fig. 3A) and the submucosal plexus (Fig. 3C) to examine a possible neuronal localization of P2X7. The staining revealed a clearly different localization of HuC/D and P2X7 in both WT and P2X7-EGFP mice, which is in agreement with previous data from transgenic mice[17]. Similar results were obtained if co-staining was performed using the anti-P2X7 nanobody, a second alternative anti-P2X7 antibody, or the anti-GFP antibody in P2X7-EGFP transgenic mice (Supplementary Fig. 3A,B). As the positive control for a neuronal expression pattern, we used antibodies against P2X2 and P2X4 receptors, which were previously shown to be expressed in enteric and other neurons[36–39]. Accordingly, the staining revealed good co-localization of HuC/D, with both receptors in distinct neuronal cell bodies (Fig. 3B). Although a uniform staining in all neurons was seen for the P2X4R, P2X2R staining appeared more variable between cells. In contrast to P2X2Rs, a punctate P2X4R staining was also detected in extraganglionic cells. Here, P2X4 co-localized with CD68, which is in agreement with its known expression in lysosomes of macrophages (Supplementary Fig. 4)[40].

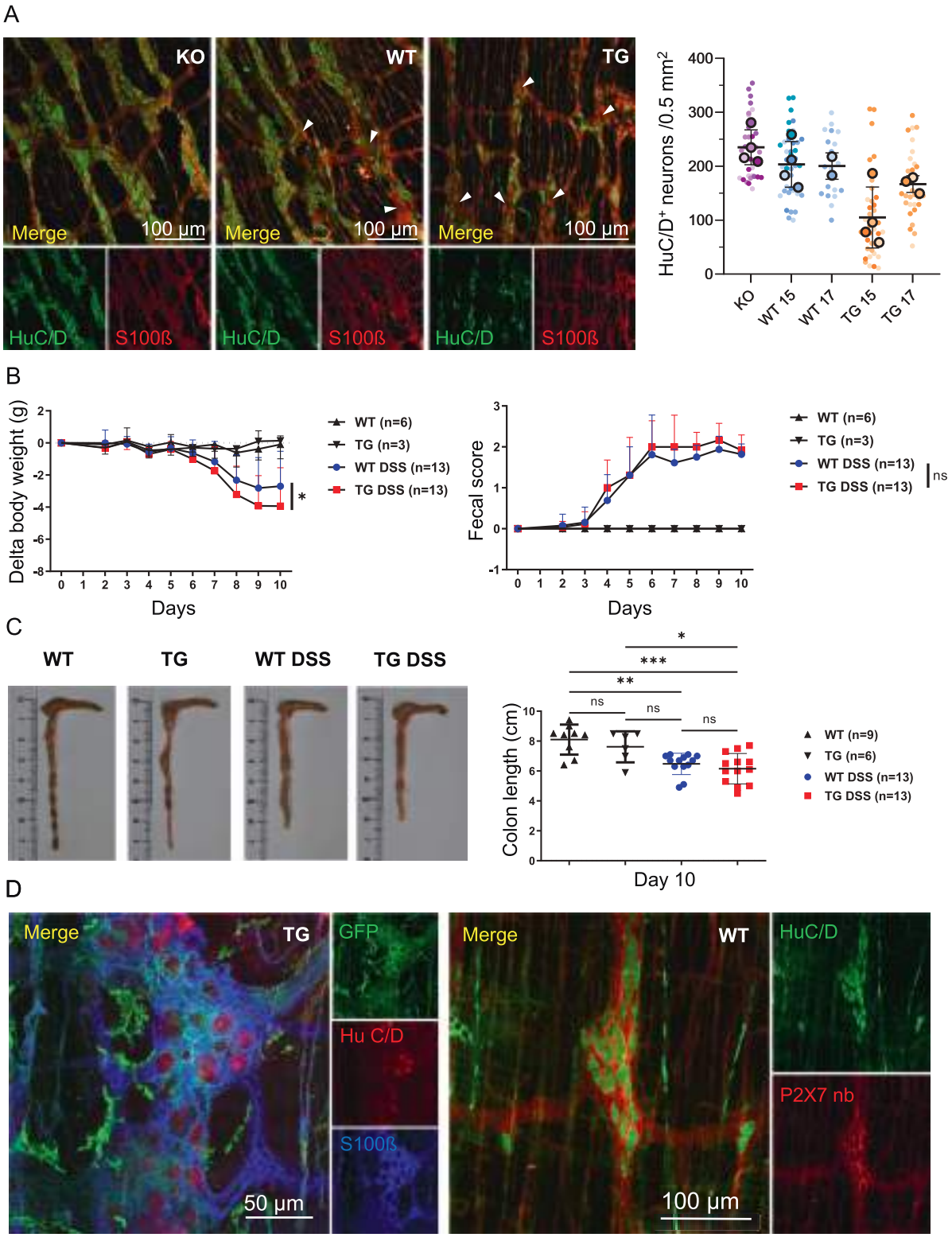
A
KO
WT
TG
Merge
100 µm
HuC/D
S100ß
HuC/D+ neurons /0.5 mm2
400
300
200
100
0
KO
WT 15
WT 17
TG 15
TG 17
B
Delta body weight (g)
Days
WT (n=6)
TG (n=3)
WT DSS (n=13)
TG DSS (n=13)
*
Fecal score
ns
C
WT
TG
WT DSS
TG DSS
Colon length (cm)
Day 10
*
***
**
ns
D
Merge
TG
GFP
Hu C/D
S100ß
50 µm
WT
HuC/D
P2X7 nb
100 µm

HuC/D is localized in the cell body; however, under pathophysiological conditions, it has been reported to show a prevalent nuclear localization[41]. Thus, to exclude the expression of P2X7 in specific neuronal substructures that are not stained with HuC/D, we also performed co-localization studies of P2X7 with β3-tubulin, which stains neuronal processes, the neuronal marker proteins PGP9.5 (protein gene product 9.5), calbindin, and calretinin (Fig. 4A), as well as with the synaptic marker proteins synaptophysin and vesicular glutamate transporter subtype 2 (Fig. 4B, Supplementary Fig. 5A). Again, none of the staining revealed a co-localization with P2X7, thus arguing against a physiological expression of P2X7 protein in enteric neurons. Our findings are supported by recent single-cell RNA sequencing studies performed on the ENS[42–44]. Based on these data, the expression of P2X7 is highest in glia, macrophages, and T cells, whereas its limited expression is only found in a minority of cells from neuronal clusters. In contrast, P2X2 is highly expressed in numerous neuronal clusters, and P2X2 and P2X7 expressions appear mutually exclusive. P2X4 is found in a variety of neuronal and nonneuronal cell types. Nevertheless, it needs to be considered that the levels of RNA transcripts do not necessarily correlate with protein levels, which can be regulated by various posttranscriptional/posttranslational processes.

Interestingly, the strong staining of the P2X7-EGFP-expressing macrophages enabled the visualization of close interactions of macrophages with the HuC/D-positive neurons (Fig. 4A), as previously described[45–47]. In addition, a close association of macrophages with blood vessels in the submucosal plexus could be observed (Fig. 3C, right panel).

Identification of P2X7 expression in enteric glia cells

Based on the previously mentioned data, we concluded that the intraganglionic P2X7-expressing cells that form the mesh-like structure in which the neurons are embedded most likely represent enteric glia cells. Enteric glia cells are generally differentiated by their localization and morphology, whereas the expression of specific marker proteins appears highly dynamic[48,49]. Using antibodies against the widely used glia marker glial fibrillary acidic protein (Fig. 5A) and S100β (S100 calcium-binding protein β) (Fig. 5B), we detected a clear co-localization of P2X7-EGFP and S100β in WT and transgenic mice. Co-localization between glial fibrillary acidic protein and P2X7 or P2X7-EGFP was less clear, most likely because of their different subcellular localization.

No induction of neuronal P2X7 expression in the dextran sulfate sodium colitis model

The previously mentioned data show a dominant expression of P2X7 in macrophages and glia cells but not in enteric neurons. This is in contrast to previous studies, where neuronal P2X7 receptors have been implicated in colitis-associated enteric neuron death[5]. Therefore, we wondered whether neuronal P2X7 expression could be induced by P2X7 activation in an *ex vivo* model, in which we incubated myenteric plexus preparations from WT, P2X7-EGFP, and *P2rx7*$^{-/-}$ mice for 60 minutes with 3 mM ATP (Supplementary Fig. 6) or 300 μM benzoyl-ATP, a more potent and specific P2X7 agonist (Fig. 6A). In agreement with previous observations[5], agonist treatment appeared to cause more neuronal cell loss in WT and in transgenic mice than in knockout mice (arrowheads in Fig. 6A and Supplementary Fig. 6), although the difference in neuron numbers was not significant (Fig. 6A). Importantly, no upregulation of P2X7 expression in neurons was observed neither in WT nor in transgenic mice (Supplementary Fig. 6). To examine a possible neuronal P2X7 upregulation under more physiological conditions and investigate whether P2X7 overexpression is associated with a higher disease susceptibility, we next subjected WT and transgenic mice to the dextran sodium sulfate (DSS) colitis model. Figs 6B and 6C show only a slightly increased weight loss of DSS-treated P2X7-EGFP mice compared with DSS-treated WT mice at day 10 but no effects on the fecal score during the entire experiment and colon length at the day of sacrifice. Likewise, swiss roll analysis did not show significant histomorphological differences between DSS-treated P2X7-EGFP mice and DSS-treated WT mice in terms of inflammation. Nevertheless, the epithelial damage appeared more pronounced in P2X7-EGFP mice (Supplementary Fig. 7). The microscopic analysis of HuC/D-stained tissue from DSS-treated mice shows no neuronal P2X7 localization (Fig. 6D). Lack of neuronal P2X7 upregulation was also confirmed in the transfer colitis model, which further demonstrated P2X7 expression in T cells, as expected (Supplementary Fig. 8).

DISCUSSION

Despite its importance as a drug target, the localization, regulation, and functions of P2X7 receptors in different cell types remain controversial. This is partly owing to the complex pharmacology of purinergic receptors and the unclear specificity of the available antibodies in different tissues. In this study, we

Fig. 6 Comparison of wild-type (WT) and P2X7-EGFP (TG) overexpressing mice in an *ex vivo* model and in the *in vivo* DSS colitis model. A, Representative images of LMMP preparations from the distal colon after treatment with 300 μM benzoyl-ATP (line 15) and statistical analysis of neuron numbers per 0.501 mm^2. Arrowheads indicate sites of neuron loss. Data from P2X7 knockout mice (KO), and two different transgenic P2X7-EGFP lines (lines 15 and 17), and their respective WT litter mates were analyzed by Brown-Forsythe and Welch analysis of variance with a post-hoc Tamhane T2 test to correct for inhomogeneity of variance. Data are represented as mean ± SEM from N = 2–4 mice per group (large symbols). Numbers from n = 9–10 images per mouse are represented in small symbols with different color intensities for each mouse. B, Delta of weight variation (left) and fecal score (right) over time in P2X7-EGFP (TG, line 17) mice and their wild-type control littermates (WT) treated or not with DSS 1% (data from 2 independent experiments). ns: not significant; *: $p < 0.05$. Fecal score: 0, normal solid feces; 1, soft feces; 2, liquid feces; 3, visible blood traces on feces. C, Pictures (left) and statistical analysis of colon length (right) at day 10 in P2X7-EGFP (TG) mice and their wild-type control littermates (WT) treated or not with DSS 1% (data from 3 independent experiments). ns: not significant; * $p < 0.05$; ** $p < 0.01$; *** $p < 0.001$. Data are represented as mean ± SD. All mice were in C57/BL6 background. Female mice of 16 weeks of age were used in (B) and (C). D, Staining of distal colon tissue from DSS-treated WT and P2X7-EGFP transgenic mice with antibodies against the neuronal marker HuC/D, the glial markers S100β, and GFP or the P2X7 nanobody, as indicated. DSS = dextran sodium sulfate; GFP = green fluorescent protein; ns = nonsignificant.

analyzed the cell type-specific P2X7 localization in the distal colon, with a focus on the myenteric plexus. We demonstrated that myenteric macrophages and enteric glia represent the dominant P2X7-expressing cell types in the myenteric plexus under both physiological and pathological conditions and visualize the close interaction of the macrophages with enteric neurons. Based on our data, we proposed that P2X7 receptors in macrophages and/or glia cells indirectly contribute to neuronal damage in colitis pathology.

P2X7 in enteric neurons and glia

The ENS and enteric glia cells have emerged as important regulators of gut barrier function and homeostasis in gastrointestinal diseases, including IBD[50]. P2X7 receptors have been described in enteric neurons[5,20,30–33], and the role of neuronal P2X7 receptors in neuronal cell death and colitis-associated motility disorders was proposed. However, the pharmacological characterization of purinergic receptor subtypes in native tissues is complex[51], and at least in the CNS, the presence of P2X7 receptors in neurons has been debated[52,53]. In this study on the myenteric plexus, using antibodies against a variety of neuronal marker proteins in distinct neuronal substructures in combination with P2X7-specific antibodies and nanobodies and *P2rx7*$^{-/-}$ mouse controls, as well as a transgenic P2X7-EGFP reporter mouse model, we could not detect neuronal P2X7 receptors. In contrast, a clear staining was found with P2X2- and P2X4-specific antibodies that were used as positive controls. Based on these data, we concluded that the P2X7 protein is either absent in enteric neurons or below the detection limit and that P2X7 receptors do not play a physiological role in enteric neurons.

Presence and function in glia cells

Enteric glia are closely associated with enteric neurons. They modulate motility, secretion, function of the epithelial barrier, and neuroinflammation and have also been involved in nociceptor sensitization and immune cell modulation[54,55]. Using both an antibody and a nanobody against P2X7, we could detect identical reticulate patterns of P2X7 staining that differed from the diffuse ganglionic background staining in *P2rx7*$^{-/-}$ mice and correlated well with the expression of the enteric glia cell marker S100β. In both WT and P2X7-EGFP reporter mice, the co-staining of P2X7 or GFP with S100β confirmed the expression in the same structures, although the expression of P2X7-EGFP appeared more irregular than that of the endogenous P2X7. The reason for this is unclear but might reflect the highly dynamic protein expression and subtype differentiation that has been reported for enteric glia[48,49]. In support of our finding, glial responses to ATP and the expression of P2X7 in enteric glia were previously reported in rats[30,56–58] and a glial cell line[59]. However, purinergic neuron to glia signaling and ATP-mediated Ca^{2+} signals in enteric glia cells were generally believed to be mediated by P2Y1 receptors[48,49,60,61]. Thus, although the importance of glia in neuroimmune interaction in colitis-associated visceral pain has recently been shown[54], the role of glial P2X7 receptors remains completely unclear. Interestingly, enteric glia in the myenteric plexus share marker proteins and functional properties with satellite glia in the dorsal root ganglia and astrocytes in the CNS, and common roles in inflammatory processes and abdominal pain generation were described[62]. Both satellite glia and Bergmann glia, a specific type of S100β-positive astrocytes, also express P2X7, suggesting common roles of P2X7 receptors in these cells. Further studies are needed to clarify the functions of glial P2X7 receptors and their involvement in colitis pathology and visceral pain.

Presence and function in macrophages

Based on their localization and specific functions, intestinal resident macrophages are classified into two major groups: the highly phagocytic lamina propria macrophages, which represent the first line of defense against pathogens and act primarily as innate immune effector cells, and the muscularis macrophages, which represent the dominant immune cell population in the muscular layer and closely and bidirectionally interact with the ENS and also with smooth muscle cells[35]. Although of different developmental origin, macrophages share many marker proteins with microglia, the resident immune cells of the CNS[63]. Muscularis macrophages resemble microglia as well morphologically and functionally[64]. P2X7 receptors are highly expressed in microglia and macrophages and staining of overexpressed P2X7-EGFP with P2X7-specific nanobodies and antibodies or antibodies against GFP resulted in a clear and detailed visualization of macrophages and revealed their close interaction with neuronal cell bodies and processes, similar to microglia in the CNS. Therefore, the P2X7-EGFP mice might provide a good model to further study these interactions. Because the maturation and release of cytokines, such as IL-1β, is the best investigated function of P2X7 receptors in macrophages, this represents the most obvious mechanism of how P2X7 could contribute not just to inflammation but also nociceptor sensitization[54]. P2X7-mediated production of reactive oxygen species[65] could further contribute to ATP-induced neuronal damage or death[5]. Because intestinal macrophages, similar to the microglia in the CNS, are considered the gatekeepers of tissue homeostasis, they are also discussed as therapeutic targets in IBD[66]. The physiological mechanism or relevance of the increased macrophage number in P2X7-EGFP mice remains to be determined, but it is reminiscent of a trend toward higher microglia numbers that were found in a preliminary analysis of the retina of P2X7-EGFP mice[34]. An intriguing possibility would be that P2X7 overexpression has an effect on macrophage migration and/or proliferation.

Involvement of P2X7 in other cell types

P2X7 receptors in other cell types besides macrophages and glia have also been involved in colitis pathology. Thus, P2X7 receptors are highly expressed in mast cells, and P2X7-mediated mast cell activation was shown to initiate and exacerbate colitis through cytokine induction and neutrophil infiltration[22]. In support of this finding, the inhibition of ATP-induced mast cell activation ameliorated colitis[23,24]. P2X7 receptors have also been involved in T-cell activation, and its expression is dynamically regulated during T-cell differentiation. T-cell subsets, including follicular helper T cells, regulatory T cells, and Th17 T cells, are sensitive to P2X7-mediated cell death[15,16], and it was reported that P2X7-mediated death of regulatory T cells decreases immune tolerance and thereby promotes inflammation[25,26]. In epithelial cells, the activation of P2X7 receptors was shown to induce IL-1β release[27], thereby suggesting promoting inflammation. Furthermore, it was shown to inhibit epithelial cell proliferation, and P2X7 receptor inhibition or deletion promoted re-epitheliation and recovery of inflammatory lesions and also enhanced tumor susceptibility[28]. Based on a study on human colonic mucosal strips, it was suggested that epithelial P2X7 receptors represent therapeutic targets for IBD[29].

In conclusion, P2X7 receptors in numerous cell types appear to contribute to colitis pathology as well as associated motility disorders and visceral sensitivity. Here, we demonstrated that in the intestinal nervous system, P2X7 receptors are dominantly expressed in macrophages and S100β-positive glia. This resembles the situation in the CNS, where P2X7 receptors are highly expressed in microglia and S100β-positive astrocytes. We proposed that P2X7 fulfills similar functions in both systems and that ATP-induced neuronal damage in the enteric system is an indirect effect of macrophage or glial P2X7 activation. Because numerous studies support beneficial effects of P2X7 blockade in central and peripheral inflammatory diseases, it represents a promising drug target, and this study provided a basis to further elucidate its cell type-specific functions and develop novel therapies.

AUTHOR CONTRIBUTIONS

Conceptualization: AN, TJ, JZ, SZ. Formal analysis: TJ, JZ, TRJ, BR, SZ, MS, FG, AN, TM, FS, BZ, PFP. Investigation: TJ, JZ, TRJ, BR, FS, BZ, PZP. Resources: FKN, SH. Writing - Original Draft: AN. Writing - Review and Editing: TJ, JZ, TRJ, SZ, MS, FG, AN, BR, TM, FKN, FS, BZ, PFP, SH. Project administration: AN. Funding acquisition: AN, MS, FG, TM, FKN, SH.

DECLARATIONS OF COMPETING INTEREST

The authors have no competing interests to declare.

FUNDING

This work was supported by funding from the Förderprogramm für Forschung und Lehre (FöFoLe) of the Ludwig-Maximilians-Universität München (No. 745/2014), the Deutsche Forschungsgemeinschaft [German Research Foundation, Project-ID: 335447717 - SFB 1328 (A3: SH, A13: TM, A15: AN, Z02: FKN, BR) and TRR-152 (P14: SZ)], and the Swiss National Science Foundation (Project number IZCNZ0-174704).

DATA AVAILABILITY

The datasets generated during and/or analyzed during this study are available from the corresponding author on reasonable request.

ACKNOWLEDGMENTS

The authors thank Barbara Kuch for technical assistance, Babett Steglich for help with scRNAseq analysis, and Yves Haufe for statistical advice.

APPENDIX A. SUPPLEMENTARY DATA

Supplementary data to this article can be found online at https://doi.org/10.1016/j.mucimm.2022.11.003.

REFERENCES

1. Orholm, M. et al. Familial occurrence of inflammatory bowel disease. *N. Engl. J. Med.* **324**, 84–88 (1991).
2. Baumgart, D. C. & Carding, S. R. Inflammatory bowel disease: cause and immunobiology. *Lancet* **369**, 1627–1640 (2007).
3. Sanchez-Munoz, F., Dominguez-Lopez, A. & Yamamoto-Furusho, J. K. Role of cytokines in inflammatory bowel disease. *World J. Gastroenterol.* **14**, 4280–4288 (2008).
4. Xavier, R. J. & Podolsky, D. K. Unravelling the pathogenesis of inflammatory bowel disease. *Nature* **448**, 427–434 (2007).
5. Gulbransen, B. D. et al. Activation of neuronal P2X7 receptor-pannexin-1 mediates death of enteric neurons during colitis. *Nat. Med.* **18**, 600–604 (2012).
6. Spear, E. T. & Mawe, G. M. Enteric neuroplasticity and dysmotility in inflammatory disease: key players and possible therapeutic targets. *Am. J. Physiol. Gastrointest. Liver Physiol.* **317**, G853–G861 (2019).
7. Niesler, B., Kuerten, S., Demir, I. E. & Schäfer, K. H. Disorders of the enteric nervous system - a holistic view. *Nat. Rev. Gastroenterol. Hepatol.* **18**, 393–410 (2021).
8. Antonioli, L., Blandizzi, C. & Giron, M. C. Enteric purinergic signaling: shaping the "brain in the gut". *Neuropharmacology* **95**, 477–478 (2015).
9. Burnstock, G. Purinergic signalling in the gut. *Adv. Exp. Med. Biol.* **891**, 91–112 (2016).
10. Diezmos, E. F., Bertrand, P. P. & Liu, L. Purinergic signaling in gut inflammation: the role of connexins and pannexins. *Front. Neurosci.* **10**, 311 (2016).
11. Gulbransen, B. D. & Sharkey, K. A. Purinergic neuron-to-glia signaling in the enteric nervous system. *Gastroenterology* **136**, 1349–1358 (2009).
12. Vuerich, M., Mukherjee, S., Robson, S. C. & Longhi, M. S. Control of gut inflammation by modulation of purinergic signaling. *Front. Immunol.* **11**, 1882 (2020).
13. Di Virgilio, F., Dal Ben, D., Sarti, A. C., Giuliani, A. L. & Falzoni, S. The P2X7 receptor in infection and inflammation. *Immunity* **47**, 15–31 (2017).
14. Di Virgilio, F., Sarti, A. C. & Grassi, F. Modulation of innate and adaptive immunity by P2X ion channels. *Curr. Opin. Immunol.* **52**, 51–59 (2018).
15. Proietti, M. et al. ATP-gated ionotropic P2X7 receptor controls follicular T helper cell numbers in Peyer's patches to promote host-microbiota mutualism. *Immunity* **41**, 789–801 (2014).
16. Rissiek, B., Haag, F., Boyer, O., Koch-Nolte, F. & Adriouch, S. P2X7 on mouse T cells: one channel, many functions. *Front. Immunol.* **6**, 204 (2015).
17. Kaczmarek-Hájek, K., Lörinczi, E., Hausmann, R. & Nicke, A. Molecular and functional properties of P2X receptors–recent progress and persisting challenges. *Purinergic Signal.* **8**, 375–417 (2012).
18. Rumney, R. M. H. & Górecki, D. C. Knockout and knock-in mouse models to study purinergic signaling. *Methods Mol. Biol.* **2041**, 17–43 (2020).
19. Antonioli, L., Blandizzi, C., Pacher, P. & Haskó, G. The purinergic system as a pharmacological target for the treatment of immune-mediated inflammatory diseases. *Pharmacol. Rev.* **71**, 345–382 (2019).
20. Evangelinellis, M. M., Souza, R. F., Mendes, C. E. & Castelucci, P. Effects of a P2X7 receptor antagonist on myenteric neurons in the distal colon of an experimental rat model of ulcerative colitis. *Histochem. Cell Biol.* **157**, 65–81 (2022).
21. Eser, A. et al. Safety and efficacy of an oral inhibitor of the purinergic receptor P2X7 in adult patients with moderately to severely active Crohn's disease: a randomized placebo-controlled, double-blind, phase IIa study. *Inflamm. Bowel Dis.* **21**, 2247–2253 (2015).
22. Kurashima, Y. et al. Extracellular ATP mediates mast cell-dependent intestinal inflammation through P2X7 purinoceptors. *Nat. Commun.* **3**, 1034 (2012).
23. Matsukawa, T. et al. Ceramide-CD300f binding suppresses experimental colitis by inhibiting ATP-mediated mast cell activation. *Gut* **65**, 777–787 (2016).
24. Ohbori, K. et al. Prophylactic oral administration of magnesium ameliorates dextran sulfate sodium-induced colitis in mice through a decrease of colonic accumulation of P2X7 receptor-expressing mast cells. *Biol. Pharm. Bull.* **40**, 1071–1077 (2017).
25. Figliuolo, V. R. et al. P2X7 receptor promotes intestinal inflammation in chemically induced colitis and triggers death of mucosal regulatory T cells. *Biochim. Biophys. Acta Mol. Basis Dis.* **1863**, 1183–1194 (2017).
26. Schenk, U. et al. ATP inhibits the generation and function of regulatory T cells through the activation of purinergic P2X receptors. *Sci. Signal.* **4**, ra12 (2011).
27. Cesaro, A. et al. Amplification loop of the inflammatory process is induced by P2X7R activation in intestinal epithelial cells in response to neutrophil transepithelial migration. *Am. J. Physiol. Gastrointest. Liver Physiol.* **299**, G32–G42 (2010).
28. Hofman, P. et al. Genetic and pharmacological inactivation of the purinergic P2RX7 receptor dampens inflammation but increases tumor incidence in a mouse model of colitis-associated cancer. *Cancer Res.* **75**, 835–845 (2015).
29. Diezmos, E. F. et al. Blockade of Pannexin-1 channels and purinergic P2X7 receptors shows protective effects against cytokines-induced colitis of human colonic mucosa. *Front. Pharmacol.* **9**, 865 (2018).
30. da Silva, M. V., Marosti, A. R., Mendes, C. E., Palombit, K. & Castelucci, P. Submucosal neurons and enteric glial cells expressing the P2X7 receptor in rat experimental colitis. *Acta Histochem.* **119**, 481–494 (2017).
31. Palombit, K., Mendes, C. E., Tavares-de-Lima, W., Barreto-Chaves, M. L. & Castelucci, P. Blockage of the P2X7 receptor attenuates harmful changes produced by ischemia and reperfusion in the Myenteric Plexus. *Dig. Dis. Sci.* **64**, 1815–1829 (2019).
32. Antonioli, L. et al. Involvement of the P2X7 purinergic receptor in colonic motor dysfunction associated with bowel inflammation in rats. *PLoS One* **9**, e116253 (2014).

33. Brown, I. A., McClain, J. L., Watson, R. E., Patel, B. A. & Gulbransen, B. D. Enteric glia mediate neuron death in colitis through purinergic pathways that require connexin-43 and nitric oxide. *Cell. Mol. Gastroenterol. Hepatol.* **2**, 77–91 (2016).
34. Kaczmarek-Hajek, K. et al. Re-evaluation of neuronal P2X7 expression using novel mouse models and a P2X7-specific nanobody. *eLife* **7**, e36217 (2018).
35. Viola, M. F. & Boeckxstaens, G. Intestinal resident macrophages: multitaskers of the gut. *Neurogastroenterol. Motil.* **32**, e13843 (2020).
36. Galligan, J. J. & North, R. A. Pharmacology and function of nicotinic acetylcholine and P2X receptors in the enteric nervous system. *Neurogastroenterol. Motil.* **16**, 64–70 (2004).
37. Ren, J. et al. P2X2 subunits contribute to fast synaptic excitation in myenteric neurons of the mouse small intestine. *J. Physiol.* **552**, 809–821 (2003).
38. Nieto-Pescador, M. G. et al. P2X4 subunits are part of P2X native channels in murine myenteric neurons. *Eur. J. Pharmacol.* **709**, 93–102 (2013).
39. Liñán-Rico, A. et al. Neuropharmacology of purinergic receptors in human submucous plexus: involvement of $P2X_1$, $P2X_2$, $P2X_3$ channels, P2Y and A_3 metabotropic receptors in neurotransmission. *Neuropharmacology* **95**, 83–99 (2015).
40. Duveau, A., Bertin, E. & Boué-Grabot, E. Implication of neuronal versus microglial P2X4 receptors in central nervous system disorders. *Neurosci. Bull.* **36**, 1327–1343 (2020).
41. Desmet, A. S., Cirillo, C. & Vanden Berghe, P. Distinct subcellular localization of the neuronal marker HuC/D reveals hypoxia-induced damage in enteric neurons. *Neurogastroenterol. Motil.* **26**, 1131–1143 (2014).
42. Zeisel, A. et al. Molecular architecture of the mouse nervous system. *Cell* **174**, 999–1014.e22 (2018).
43. Morarach, K. et al. Diversification of molecularly defined myenteric neuron classes revealed by single-cell RNA sequencing. *Nat. Neurosci.* **24**, 34–46 (2021).
44. Drokhlyansky, E. et al. The human and mouse enteric nervous system at single-cell resolution. *Cell* **182**, 1606–1622.e23 (2020).
45. Gabanyi, I. et al. Neuro-immune interactions drive tissue programming in intestinal macrophages. *Cell* **164**, 378–391 (2016).
46. Muller, P. A. et al. Crosstalk between muscularis macrophages and enteric neurons regulates gastrointestinal motility. *Cell* **158**, 300–313 (2014).
47. Phillips, R. J. & Powley, T. L. Macrophages associated with the intrinsic and extrinsic autonomic innervation of the rat gastrointestinal tract. *Auton. Neurosci.* **169**, 12–27 (2012).
48. Boesmans, W., Lasrado, R., Vanden Berghe, P. & Pachnis, V. Heterogeneity and phenotypic plasticity of glial cells in the mammalian enteric nervous system. *Glia* **63**, 229–241 (2015).
49. Gulbransen, B. D. & Sharkey, K. A. Novel functional roles for enteric glia in the gastrointestinal tract. *Nat. Rev. Gastroenterol. Hepatol.* **9**, 625–632 (2012).
50. Sharkey, K. A., Beck, P. L. & McKay, D. M. Neuroimmunophysiology of the gut: advances and emerging concepts focusing on the epithelium. *Nat. Rev. Gastroenterol. Hepatol.* **15**, 765–784 (2018).
51. Anderson, C. M. & Nedergaard, M. Emerging challenges of assigning P2X7 receptor function and immunoreactivity in neurons. *Trends Neurosci.* **29**, 257–262 (2006).
52. Illes, P., Khan, T. M. & Rubini, P. Neuronal P2X7 receptors revisited: do they really exist? *J. Neurosci.* **37**, 7049–7062 (2017).
53. Miras-Portugal, M. T., Sebastián-Serrano, Á., de Diego García, L. & Díaz-Hernández, M. Neuronal P2x7 receptor: involvement in neuronal physiology and pathology. *J. Neurosci.* **37**, 7063–7072 (2017).
54. Grubišić, V. et al. Enteric Glia Modulate Macrophage Phenotype and Visceral Sensitivity following Inflammation. *Cell Rep.* **32**:108100.
55. Wang, H., Foong, J. P. P., Harris, N. L. & Bornstein, J. C. Enteric neuroimmune interactions coordinate intestinal responses in health and disease. *Mucosal Immunol.* **15**, 27–39 (2022).
56. Mendes, C. E., Palombit, K., Tavares-de-Lima, W. & Castelucci, P. Enteric glial cells immunoreactive for P2X7 receptor are affected in the ileum following ischemia and reperfusion. *Acta Histochem.* **121**, 665–679 (2019).
57. Van Crombruggen, K., Van Nassauw, L., Timmermans, J. P. & Lefebvre, R. A. Inhibitory purinergic P2 receptor characterisation in rat distal colon. *Neuropharmacology* **53**, 257–271 (2007).
58. Vanderwinden, J. M., Timmermans, J. P. & Schiffmann, S. N. Glial cells, but not interstitial cells, express P2X7, an ionotropic purinergic receptor, in rat gastrointestinal musculature. *Cell Tissue Res.* **312**, 149–154 (2003).
59. Bhave, S. et al. Connexin-purinergic signaling in enteric glia mediates the prolonged effect of morphine on constipation. *FASEB J.* **31**, 2649–2660 (2017).
60. Boesmans, W. et al. Neurotransmitters involved in fast excitatory neurotransmission directly activate enteric glial cells. *Neurogastroenterol. Motil.* **25**, e151–e160 (2013).
61. Gomes, P. et al. ATP-dependent paracrine communication between enteric neurons and glia in a primary cell culture derived from embryonic mice. *Neurogastroenterol. Motil.* **21**, 870–e62 (2009).
62. Morales-Soto, W. & Gulbransen, B. D. Enteric glia: a new player in abdominal pain. *Cell. Mol. Gastroenterol. Hepatol.* **7**, 433–445 (2019).
63. Ginhoux, F. & Prinz, M. Origin of microglia: current concepts and past controversies. *Cold Spring Harb. Perspect. Biol.* **7**:a020537.
64. Verheijden, S., De Schepper, S. & Boeckxstaens, G. E. Neuron-macrophage crosstalk in the intestine: a "microglia" perspective. *Front. Cell. Neurosci.* **9**, 403 (2015).
65. Kopp, R., Krautloher, A., Ramírez-Fernández, A. & Nicke, A. P2X7 interactions and signaling - making head or tail of it. *Front. Mol. Neurosci.* **12**, 183 (2019).
66. Na, Y. R., Stakenborg, M., Seok, S. H. & Matteoli, G. Macrophages in intestinal inflammation and resolution: a potential therapeutic target in IBD. *Nat. Rev. Gastroenterol. Hepatol.* **16**, 531–543 (2019).
67. Dieleman, L. A. et al. Chronic experimental colitis induced by dextran sulphate sodium (DSS) is characterized by Th1 and Th2 cytokines. *Clin. Exp. Immunol.* **114**, 385–391 (1998).